A study of R-phase transition and temperature memory effect in a commercial Nitinol wire

N. M. LOHAN, E. MIHALACHE, B. PRICOP, M.G. SURU, L.G. BUJOREANU[*]
Faculty of Materials Science and Engineering, The "Gheorghe Asachi" Technical University of Iaşi, Bd. D. Mangeron 67, 700050 Iaşi, Romania

Ni-Ti shape memory alloys (SMAs) commercially designated as NITINOL represent, up to present date, the most intensely studied SMAs. Due to this fact, commercial applications have been developed under various forms, such as tubes, rods, wires, etc. The present study examines the behaviour of a $Ni_{47.4}Ti_{52.6}$ commercial wire with 0.5 mm diameter. By means of a Differential Scanning Calorimeter (DSC), various wire samples were subjected to thermal cycles, with the aim to emphasise heat flow variations during the reversible martensitic transformation. Considering that R-phase transition is a competitive phenomenon with regards to martensitic transformation, the DSC cycles aimed to supress the latter in order to enhance the former. On the other hand, the interruption of reverse martensitic transformation caused the occurrence of temperature memory effect, consisting in the splitting into two parts of the martensite reversion from the subsequent thermal cycle. The evolution of DSC thermograms was corroborated with structural analyses performed by X-Ray diffraction (XRD). For this purpose, the samples were subjected to the same heat treatments as during DSC thermal cycles.

1. Introduction

Since the discovery of their unique properties, SMAs have been used for a wide variety of applications. NiTi SMAs are currently presenting notable interest in engineering, as well as technical and medical applications. The combination between good biocompatibility [1], ductility [2] and strength [3] with specific functional properties like the shape memory effect (SME) [4] and superelasticity (SE) [5, 6] creates an exceptional material for applications such as biomedical implants or medical device [7], actuators and micro-controllers [8] or roller bearings [9]. The functional properties of NiTi SMAs are due to a reversible martensite phase change.

Generally, on heating, the reverse martensitic transformation results between monoclinic B19' type crystal structure (martensite -M) and cubic B2 type crystal structure (austenite - A) [10]. In some cases, upon the cooling of NiTi SMAs, is possible to observe the formation of an intermediate rhombohedral phase, between A and M, called R-phase [11]. The occurrence of the R-phase was explained by the presence of precipitates, mainly Ti_3Ni_4 [12]. R-phase transition was described as a kind of martensite transformation (actually pre-martensitic) with small thermic hysteresis [13].

The most effective way to reveal the presence of R-phase transition is by means of Differential Scanning Calorimetry (DSC) which enables the occurrence of an additional exothermic maximum on DSC charts recorded during cooling, especially in annealed and aged Ni-rich equiatomic alloys [14].

Another important phenomenon commonly observed in NiTi based SMAs - besides SME, SE and two way shape memory effect (TWSME) – is the so called temperature memory effect (TME) [15]. TME consists in the formation of two martensite "populations" [16], as an effect of the interruption of martensite reversion and the occurrence of two-stage reverse martensitic transformation during the heating in subsequent cycle [17].

Since both these phenomena are noticeable in NiTi SMAs, one would expect that the study of their interaction and eventual relationships would be one of the popular research topics within the endeavour to contribute to the development of these unique materials. However, no reports can be found in literature concerning the conjugated occurrence and conditioning terms of these phenomena, specific for NiTi SMAs.

The purpose of the present paper is to study the relationship between R-phase transition and TME within commercial wires of NiTi SMA, commonly named NITINOL, according to the symbols of chemical elements and the initials of the institution (Naval Ordnance Laboratory) where these alloys were first developed [18].

2. Materials and methods

A commercial 0.5 mm-diameter NITINOL wire was purchased, with chemical composition $Ni_{47.4}Ti_{52.6}$, which was martensitic at room temperature. Up to 5-mm long wire fragments were cut, weighing less than 10 mg, for differential scanning calorimetry (DSC) experiments.

For this purpose, a NETZSCH differential scanning calorimeter type DSC 200 F3 Maya was used, with

sensitivity: < 1 W, temperature accuracy of 0.1 K and enthalpy accuracy—generally <1%. The device was calibrated with Bi, In, Sn, and Zn standards. Temperature scans were performed between 283 and 393 K, with 10 K/min, under Ar protective atmosphere and liquid nitrogen cooling was used to obtain a constant cooling rate.

A part of NITINOL wire was heat treated, as it will be shown later, in order to enable the formation of R-phase.

Both as delivered (initial) and heat treated wires were cut into 10 mm-long fragments. Ten such fragments were compactly laid on flat rectangular surfaces and embedded into cold mounting acrylic resin [19]. After reticulation, arrays of ten parallel wires were obtained, both in initial and heat treated conditions. These metallographic specimens were carefully ground and polished, before being subjected to X-ray (XRD) diffraction studies.

XRD patterns were recorded, on 2θ range from 20 to 90^0, using a D8 Advance - Bruker AxS GmbH diffractometer with Cu-Kα radiation to determine phase structure. For this purpose, the lattice parameters found in 00-035-1281 crystallographic database and the literature dedicated to XRD study of R-phase transition [20] were considered, as summarized in Table 1.

Table 1 Crystallographic data within the studied region of 2θ angle, according to 00-035-1281 database and [20]

2θ	d	h	k	l	Phase
^{0}	nm				
38.2351	0.2352	1	0	1	B19'
38.9405	0.2311	1	1	0	B19'
39.2231	0.2295	0	2	0	B19'
41.3645	0.2181	1	-1	1	B19'
42.176	0.2141	0	0	1	R-phase
42.354	0.2132	1	1	0	B2
42.61	0.212	-1	0	1	R-phase
43.9165	0.206	0	0	2	B19'
44.9266	0.2016	1	1	1	B19'
45.1867	0.2005	0	2	1	B19'

3. Results and discussion

The first DSC thermograms illustrate stabilized heat flow variation during two complete heating-cooling cycles between 283 and 393 K, as shown in Fig.1.

Considering the specimen as martensitic at room temperature, the endothermic peak observed during heating can be associated with martensite (B19') reversion to parent (B2) phase [21]. The critical transformation temperatures were determined with 0.1 K accuracy, by "tangent method" [22] as A_s = 351.5 K and A_f = 363.8 K, for the start and the finish of reverse martensitic transformation, respectively. During cooling, two exothermic peaks are noticeable. The former of these maxima can be ascribed to R-phase transition, with critical temperatures R_s = 332.7 K and R_f = 324.5 K, and latter to forward (direct) martensitic transformation [23], which be began at M_s = 320.3 K and M_f = 304.5 K. All of the three peaks are perfectly reproducible in the second cycle [24].
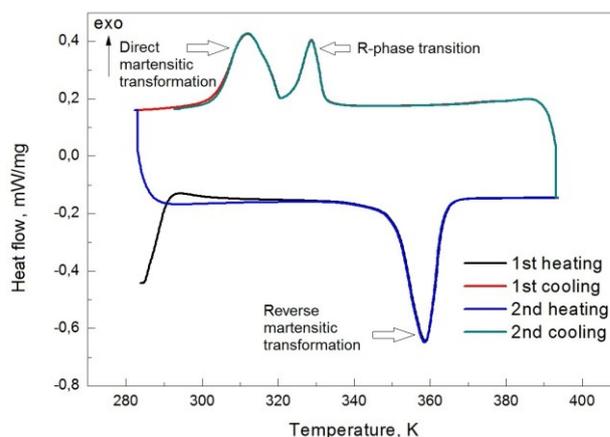

Fig.1 Heat flow variation during two stabilized heating-cooling cycles of the wire specimen in initial condition, revealing a reversible martensitic transformation and R-phase transition

In order to reveal the occurrence of TME, the reverse martensite transformation was interrupted, the following cooling was performed to completion and the splitting of endothermic peak was obtained during subsequent heating, as illustrated on the DSC thermogram in Fig.2.
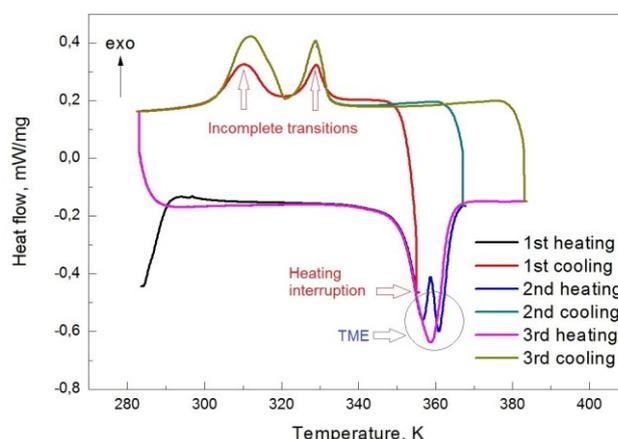

Fig.2 Heat flow variation during heating arrest before the completion of martensite reversion, causing the occurrence of temperature memory effect in subsequent heating cycle

After heating interruption at 355 K, Fig.2 shows that the following cooling, down to 283 K, was accompanied by smaller exothermic peaks for both incomplete R-phase and direct martensitic transformations. The corresponding transformation temperatures were determined as: R_s = 332.0 K, R_f = 325.3 K, M_s = 316.6 K and M_f = 303.7 K. This evolution suggests that, during incomplete heating, only a small amount of parent phase was formed and for this reason, during subsequent cooling, both exothermic transformations were diminished as compared to complete ones. Considering that a certain "population" of martensite plates did not reverse to parent phase, due to heating

interruption at 355 K, it can be assumed that the splitting of endothermic peak, during the subsequent complete heating cycle, could be the evidence of TME occurrence [25]. The temperatures of the two endothermic peaks are 356.8 K and 361 K but this behaviour could be repetitive [26]. It is noticeable that, in the third complete cooling-heating cycle, both forward and reverse transformations were produced with the same intensities and within then same critical temperatures as shown in Fig.1.

Next DSC experiments aimed to disclose the occurrence of R-phase transition, considering that it is antagonistic with martensite transformation [27]. When thermal cycling was performed by avoiding both forward and reverse martensitic transformations, a reversible R-phase transition appeared on DSC thermograms. Thus, Fig.3 displays an intermediary endothermic peak, associated with reverse R-phase transition on heating, the entire reversible transition being shown by a hatched area.
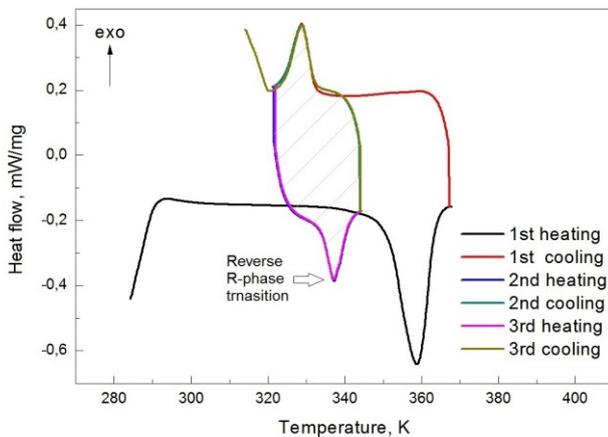

Fig.4 Heat flow variations emphasizing the absence of TME during R-phase transition

During second-cycle cooling, direct R-phase transition occurred again, between $R_s = 332.1$ K and $R_f = 324.7$ K, being almost unaltered by the interruption. Moreover, during third-cycle heating up to 345 K, the reverse R-phase transition was observed, between $R_{sh} = 334.3$ K and $R_{fh} = 341.1$ K, without any evidence of splitting the endothermic peak associated with this transition. During third-cycle cooling, direct R-phase transition is noticed without any change, demonstrating that this transformation is insensible to heating interruptions. The antagonistic character of both R-phase and martensitic transformations is proved again, during fourth-cycle heating to 367 K. Thus, after the occurrence of reverse R-phase transition, between $R_{sh} = 334.3$ K and $R_{fh} = 341.1$ K, martensite reversion was noticed with very low intensity, as pointed out by the arrow, between $A_s = 355.3$ K and $A_f = 361.1$ K. So, it can be assumed that the occurrence of reverse R-phase transition hindered the following martensite reversion to parent phase. Nevertheless during fourth-cycle cooling down to 283 K, both direct R-phase and martensite transitions occurred with unchanged intensities and in unchanged position, between $R_s = 332.4$ K and $R_f = 324.7$ K and between $M_s = 320.4$ K and $M_f = 303.9$ K, respectively.

The final series of four DSC thermal cycles was applied with the aim to emphasize the effects of direct martensitic interruption, on R-phase, as illustrated in Fig.5.

After the first heating to 367 K, martensite reversion occurred in stabilized position, between $A_s = 351.9$ K and $A_f = 363.2$ K. First-cycle cooling enabled direct R-phase transition between $R_s = 332.3$ K and $R_f = 324.8$ K and the begging of direct martensitic transformation at $M_s = 319.9$ K. The first incomplete direct martensitic transformation (IM-1) was interrupted at 317 K. During second-cycle heating, incomplete reverse R-phase transition was pointed up, between $R_{sh} = 334.2$ K and $R_{fh} = 340.7$ K, by an endothermic peak with lower intensity as compared to those noticed in Figs. 3 and 4.

Fig.3 Heat flow variation revealing perfectly reversible R-phase transition (hatched area)

After a first complete heating cycle, accompanied by martensite reversion to parent phase between $A_s = 351.6$ K and $A_f = 363.5$ K, cooling was interrupted at 321 K, after R-phase transition occurred between $R_s = 332.4$ K and $R_f = 324.7$ K and the forward martensitic transformation was avoided. For this reason, the subsequent heating, up to 347 K, enabled the occurrence of reverse R-phase transition, between critical temperatures $R_{sh} = 334.2$ K, $R_{fh} = 341.1$ K. In the following cooling-heating cycles, the perfectly reversible character of R-phase transition was demonstrated by the stability of corresponding exothermic and endothermic peaks in such a way that the critical transformation temperatures have been unchanged.

In the four thermal cycles performed according to Fig.4, an attempt was made to reveal the occurrence of TME within R-phase transition. For this purpose, an initial heating was applied up to 367 K and martensite reversion to parent phase occurred between $A_s = 351.4$ K and $A_f = 363.4$ K. Next cooling was applied down to 321 K enabling direct R-phase transition, between $R_s = 332.4$ K, $R_f = 324.7$ K. Second-cycle heating was interrupted at 337 K, after the initiation of reverse R-phase transition, at $R_{sh} = 334.3$ K.
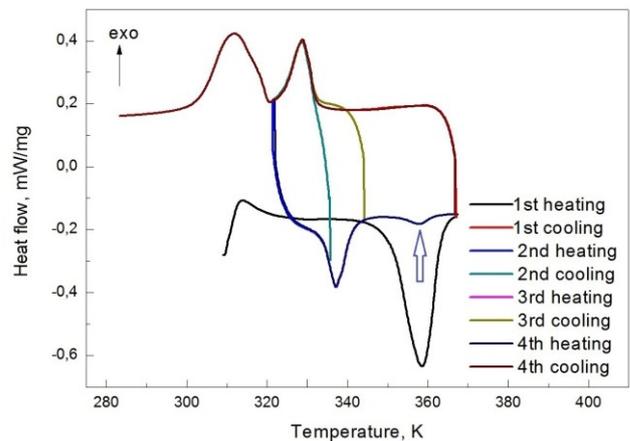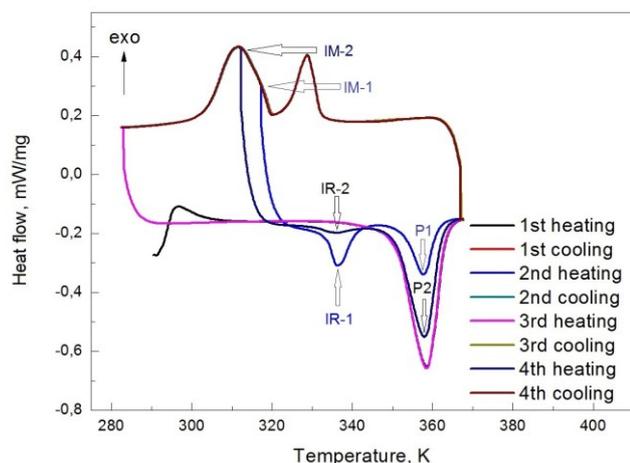
Fig.5 Heat flow variations emphasizing the competition between martensitic transformation and R-phase transition

Table 2 Temperature corresponding to the formation of 50% transformed phase (K)

	Fig.1	Fig.2	Fig.3	Fig.4	Fig,5
M_{50}	312.2	312.2	-	312.0	311.9
R_{c50}	329.0	329.0	329.1	328.9	328.9
R_{h50}	-	-	337.4	337.3	336.4
A_{50}	358.9	358.9	358.9	358.7	358.7
A_{TME1}	-	356.8	-	-	-
A_{TME2}	-	361.0	-	-	-

It is obvious that the reversible martensitic transformation has been very stable: the temperature of martensite formation was located at M_{50} =311.9 - 312.2 K and that of its reversion at A_{50} = 358.7 – 358.9 K. R-phase transition, when completed, occurred between R_{c50} = 329 ± 0.1 K and R_{h50} = 337.3-337.4 K. These values prove the unique thermal stability of R-phase transition.

The structural analysis of NITINOL wire specimens, in initial and heat treated states, was performed by scanning electron microscopy (SEM) and XRD.

On SEM micrographs no martensite plates have been noticeable, after etching, even with aggressive solutions such as 2.2% $K_2S_2O_5$ and 0.8% NH_4HF_2 in 100 ml aqueous solution.

A wire segment was heated to 370 K, maintained 300 s, cooled in furnace until 333 K, then it was water quenched, in order to retain R-phase. The XRD patterns of the two specimen conditions are shown in Fig. 6.
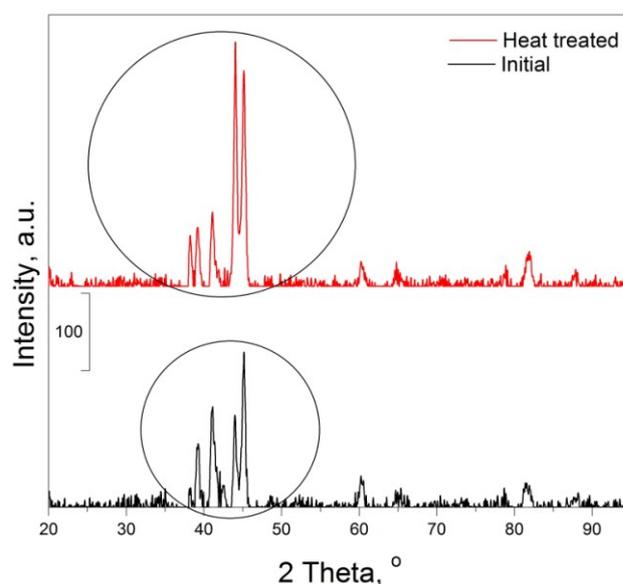
This incompleteness of reverse R-phase transition enabled an incomplete reverse martensitic transformation to parent phase (P1), between A_s = 353.6 K and A_f = 361.4 K. This is a new evidence of the competition between reverse R-phase and martensitic transformation. During second-cycle cooling, both direct R-phase and martensitic transitions were observed in unchanged positions with the same intensities as in Figs. 1, 2 and 4. For this reason, the third-cycle heating caused a reverse martensitic transformation and an endothermic peak identical to those observed in all previous DSC thermograms. This means that, if thermal cycling is complete, the alloy behaves in a stabilized manner, no matter what interruptions were previously done. In order to verify this feature, the direct martensitic transformation was interrupted at 312 K, in a more advanced stage (IM-2), in third-cycle cooling. Since direct martensitic transformation occurred in a proportion of almost 50 %, the reverse R-phase transition (IR-2) was almost inexistent. However, this hindrance of R-phase transition supported the development, during fourth-cycle heating, of martensite reversion to parent phase (P2) in a more significant manner as compared to P1. Despite this lower intensity of martensite reversion, during fourth-cycle cooling both direct transformations (R-phase and martensitic) were observed unaltered, from the point of view of intensity and thermal range. A summary of the temperatures corresponding to the formation of 50% transformed phase (the peaks of DSC exothermic maxima or endothermic minima), determined from Figs. 1-5, is shown in Table 2. During heating, these endothermic maxima are R_{h50} and A_{50} for R-phase transition and martensite reversion, respectively. In addition, the two minima caused by TME are designated as A_{TME1} and A_{TME2}. During cooling, the exothermic maxima corresponding to R-phase transition and martensite forward (direct) transformation are R_{50} and M_{50}.

Fig.6 XRD patterns of wire specimens in initial and heat treated (370 K/ 300s/ furnace/ 333K/ water) conditions

The diffraction maxima were indexed, considering the data listed in Table 1. The results, including quantitative analysis of phase amounts, are given in Table 3.

Table 3 Crystallographic parameters determined from XRD patterns from Fig.6

Phase	Initial		Heat treated	
	2θ, °	%	2θ, °	%
B19'(101)	38.22	3.0	38.22	7.5
B19'(020)	39.16	13.1	39.16	8.7
B19'(1$\bar{1}$1)	41.1	22.7	41.1	10.9
R(001)	-	--	41.92	2.5
B2(110)	42.44	5.0	-	-
R($\bar{1}$01)	-	-	42.66	2.7
B19'(002)	44	20.9	44.06	36.0
B19'(021)	45.16	35.2	45.16	31.8

For a better insight of the changes induced by heat treatment, the central regions of the two XRD patterns, marked by circles and comprising five main diffraction maxima, were magnified and overlapped, as shown in Fig.7.
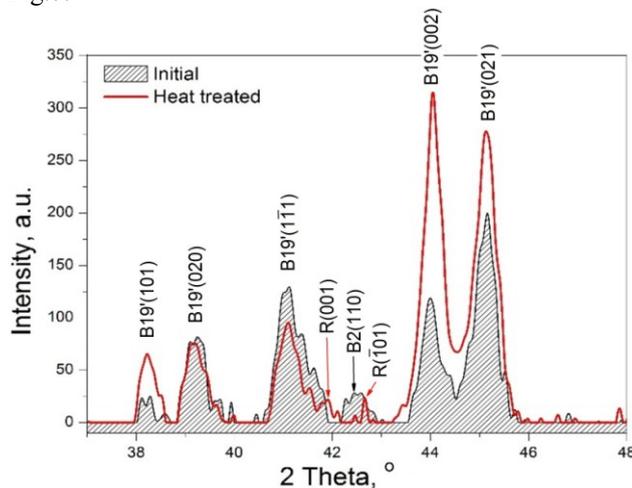

Fig.7 Magnified XRD patterns of the wire specimens in initial and heat treated conditions, emphasizing the changes induced by heat treatment.

The occurrence of R-phase diffraction maxima is typically noticed as an effect of the splitting of (110) main diffraction maximum of B2 parent phase [28]. In the case of Ti-rich NiTi alloys, this effect is more obvious and the two emerging R-phase maxima are (001) and ($\bar{1}$01) [29]. The intensities of the two R-phase maxima are rather reduced but this can be an effect of test temperature. The present XRD patterns were recorded at room temperature and the occurrence of R-phase transition is enhanced by low temperatures [30].

By cumulating the quantitative results listed in Table 3, it follows that the wire specimen contained, in initial state, a relative amount of 95 % B19' martensite and 5 % B2 parent phase, while the heat treated state had 94.8 % martensite and 5.2 % R-phase. It appears that all parent phase transformed to R-phase, as an effect of heat treatment.

4. Summary and conclusions

A commercial $Ni_{47.4}Ti_{52.6}$ wire, which is martensitic at room temperature, was subjected to thermal cycling performed by means of a DSC device.

In initial condition, the wire specimens experienced martensite reversion to parent phase, during heating, between $A_s = 352$ K and $A_f = 363$ K. During heating, R-phase transition occurred between $R_s = 332$ K and $R_f = 325$ K followed by direct (forward) martensitic transformation between $M_s = 320$ K and $M_f = 304$ K.

Temperature memory effect (TME) was caused by an incomplete heating cycle, performed with heating interruption between A_s and A_f critical temperatures. TME did not occur after the interruption of neither R-phase transition nor direct martensitic transformation.

Each time martensite transformation was impeded to occur completely R-phase transition was observed both during cooling and heating. When thermal cycling was performed between the critical temperatures $M_s = 320$ K and $A_s = 352$ K, a reversible R-phase transition was noticeable. The critical temperatures of this transition were $R_s = 332$ K and $R_f = 325$ K, during cooling and $R_{sh} = 334$ K and $R_{fh} = 341$ K, during heating.

References

[1] M. Mirjalili, M. Momeni, N. Ebrahimi, M.H. Moayed, Mat Sci Eng C, **33** 2084 (2013).
[2] S.K. Wu, H.C. Lin, J Alloy Compd **355** 72 (2003).
[3] K. Otsuka, X. Ren, Prog Mater Sci **50,** 511 (2005).
[4] J. Van Humbeeck, Shape Memory Alloys: A Material and a Technology, Advanced Engineering Materials 2001, 3, No. 11.
[5] A.R. Pelton, G.H. Huang, P. Moine, R. Sinclair, Mat Sci Eng A **532** 130 (2012).
[6] T.W. Duerig, D.E. Tolomeo, M. Wholey, Minim Invas Ther **9** 235 (2000).
[7] A. Biesiekierski, J. Wang, M. A-H. Gepreel, C. Wena, Acta Biomater **8** 1661 (2012).
[8] J. Mohd Jani, M. Leary, Al. Subic, M. A. Gibson, Mater Design **56** 1078 (2014).
[9] W. Predki, A. Knopik, B. Bauer, Mat Sci Eng A **481–482** 598 (2008).
[10] J. Olbricht, A. Yawny, J. L. Pelegrina, G. Eggeler, V. A. Yardley, J Alloy Compd **579** 249 (2013).
[11] K. Otsuka, Engineering Aspects of Shape Memory Alloys, T. W. Duerig, K. N. Melton, D. Stökel, C. M. Wayman (Eds.), Butterworth-Heinemann, p. 36 (1990).

[12] T. Fukuda, A. Deguchi, T. Kakeshita, T. Saburi,
     Mater Trans JIM **38**(6) 514 (1997).
[13] Y. Zhou, G. Fan, J. Zhang, X. Ding, X. Ren, J. Sun,
     K. Otsuka, Mat Sci Eng A **438–440** 602 (2006).
[14] L. G. Bujoreanu, M. L. Young, S. Gollerthan,
     C. Somsen, G. Eggeler, Int J Mater Res
     101(5) 623 (2010).
[15] Y. J. Zheng, L. S. Cui, Acta Metall Sin
     40, 915 (2004).
[16] K. Madangopal, S. Banerjee, S. Lele, Acta Metall
     Mater **42**, 1875 (1994).
[17] Z.G. Wang, X.T. Zu, S. Zhu, L.M. Wang, Mater Lett
     59 491 (2005).
[18] K. N. Melton, Engineering Aspects of Shape Memory
     Alloys, T. W. Duerig, K. N. Melton, D. Stökel,
     C. M. Wayman (Eds.), Butterworth-Heinemann,
     p. 21 (1990).
[19] N. Cimpoeşu, S. Stanciu, I. Doroftei, I. Ioniţă,
     V. Radu, P. Paraschiv, Optoelectron Adv Mater –
     Rapid Comm. **4**(12) 2028 (2010).
[20] X. B. Wang, B. Verlinden and J. Van Humbeeck,
     Mater Sci Tech-Lond, **30** (13a) 1517 (2014).
[21] M. Branco, L. Guerreiro, K.K. Mahesh, F.M. Braz
     Fernandes, Constr Build Mater **36** 508 (2012).
[22] N. M.Lohan, B. Pricop, L. G. Bujoreanu,
     N. Cimpoesu, Int J Mater Res **102(11)** 1345 (2011).
[23] K.K. Mahesh, F.M. Braz Fernandes, R.J.C. Silva,
     G. Gurau, Phys Proced **10** 22 (2010).
[24] M. F.-X. Wagner, S. R. Dey, H. Gugel, J. Frenzel,
     C. Somsen, G. Eggeler, Intermetallics
     18 1172 (2010).
[25] G. Vitel, A. L. Paraschiv, M. G. Suru, N. Cimpoesu,
     L.-G. Bujoreanu, Optoelectron Adv Mater. –
     Rapid Comm., **5(8)**, 858 (2011).
[26] Yanjun Zheng, Juntao Li, Lishan Cui, Mater Letters
     63 949 (2009)
[27] G. Helbert, L. Saint-Sulpice, S. A. Chirani, L. Dieng,
     T. Lecompte, S. Calloch, P. Pilvin, Mech Mater,
     79 85 (2014).
[28] J. Uchil, F.M. Braz Fernandes, K.K. Mahesh, Mater
     Charact **58** 243 (2007).
[29] K. Harikrishnan, K. Chandra, P. S. Misra, Vinod S.
     Agarwala, ESOMAT 2009 02018 (2009).
[30] F.M. Braz Fernandes, K.K. Mahesh, R.M.S. Martins,
     R.J.C. Silva, C. Baehtz, J. von Borany, Mater Charact
     76, 35 (2013).

_____

*Corresponding author: lgbujor@tuiasi.ro